JOURNAL OF PROPULSION AND POWER
Vol. 26, No. 1, January–February 2010

Technical Notes

Isolator/Combustion Chamber Interactions During Supersonic Combustion

Qiuya Tu* and Corin Segal†
University of Florida, Gainesville, Florida 32611

DOI: 10.2514/1.46156

Nomenclature

A_1 = entrance area, m^2
D = hydraulic diameter, m
F_1 = entrance stream thrust
f_1 = nondimensional stream thrust parameter
g_1 = nondimensional enthalpy parameter
H_0 = stagnation enthalpy at the entrance, kJ
h = step height, 12.5 mm
M_1 = entrance Mach number
P_r = pressure ratio
p = pressure, Pa
Re_θ = Reynolds number
X = axial distance, m
θ = momentum thickness

Introduction

THE isolator, which in most cases plays only the role of protecting the inlet flow from adverse backpressure, adds weight, internal drag and heat loads on the engine structure; therefore, its length must be limited to the minimum necessary required by operability constraints [1]. The isolator can be viewed as an extension of the inlet where additional compression takes place, but its purpose serves the distinct function of protecting the inlet flow from the adverse effects of combustion pressure rise. Boundary layers are present in the isolator after having formed on the long vehicle forebody and inlets surfaces. The interaction between the boundary layer and adverse pressure gradient may result in flow separation and formation of shock waves. The flowfield in the isolator shown in Fig. 1 represents the case in which compression is achieved both through an oblique shock train in the supersonic region 1 and through area expansion of the subsonic flow in region 2. Near the wall, in region 3, a separation bubble forms to balance the pressure gradient across the isolator length through the shear stress [2]. A repeated shock structure follows in the core of the duct. This flow structure establishes the combustion chamber entrance conditions, where it further interacts with the heat release effects determining the flow stability and the process efficiency. The oblique shock train shown in Fig. 1 is characteristic for a higher Mach number operation. For a moderate Mach number at the isolator entrance or a relatively thick boundary layer, a weaker train of oblique shocks takes place in the form of a set of bifurcated shocks, with the subsonic region 2 achieving a gradual compression in the isolator [3,4]. In both cases, the shock train must ensure that the initial wave does not propagate upstream into the inlet to disrupt the flow or, in the limit, result in the inlet unstart.

As a result of the formation of the shock train structure, the issue of immediate interest is the prediction of the minimal isolator length that can be allowed; a second issue of great importance is the losses related to the isolator drag. Once the isolator is sized, a critical issue is the shock train stability as the engine undergoes transients.

The isolator length can be determined, at nominal design conditions, by the pressure rise that must be achieved between the inlet outlet and the combustion chamber entrance. This requirement, written in normalized parameters [2], depends on the pressure ratio, $p_r = p_{\text{out}}/p_{\text{in}}$, as follows:

$$\frac{X}{D_H} = \frac{1}{4K}\frac{g_1^2}{\gamma f_1}\left[\frac{p_r - 1}{(f_1 - p_r)(f_1 - 1)} + \frac{1}{f_1}\ln\frac{p_r(f_1 - 1)}{(f_1 - p_r)}\right] + \frac{\gamma - 1}{2\gamma}\ln p_r \tag{1}$$

where $4K$ is the constant friction coefficient at the duct entrance, taken as 44.5; D_H is the hydraulic diameter, $4 \times$ area/duct perimeter; $f_1 = \frac{F_1}{p_1 A_1}$, where F is the stream thrust, A is the area, and the subscript refers to the isolator-entrance station; and $g_1 = \frac{\dot{m}\sqrt{(\gamma-1)H_0}}{p_1 A_1}$, where H_0 is the stagnation enthalpy at the duct entrance.

Equation (1) was found to predict the shock train length accuracy with 20% over a broad range of experimental results, including ducts of various shapes (round and rectangular), entrance Mach numbers ranging from 1.5 to 5, order of magnitude variation in the entrance Reynolds number, and different friction coefficients.

An additional correlation was offered by Waltrup and Billig [5] based on experimental data for a circular duct, as shown in the following equation,

$$\frac{X}{\sqrt{D}} = \frac{\theta^{1/2}}{Re_\theta^{1/4}}\frac{1}{M_1^2 - 1}[50(p_r - 1) + 170(p_r - 1)^2] \tag{2}$$

which emphasizes the dependence of the shock train length on the Reynolds number, Re_θ, the boundary layer momentum thickness, θ, and the isolator entrance Mach number, M_1. Equation (2) indicates that, for a fixed pressure ratio, the shock train length increases for flows with shock boundary layers at the isolator entrance and decreases with increased Reynolds and Mach numbers. Thicker boundary layers separate under weaker shock waves, and a smaller angle of the initial shock wave results in a long shock train. As the Reynolds number increases, the boundary layer can withstand stronger shocks and the angle of the initial shock that generates the separation is more abrupt, resulting in a shorter shock train. The Mach number effect is not immediately evident from the equation because it is coupled to the pressure ratio. As the Mach number increases, the required compression that would lead to separation is higher. The angle of the shock wave that leads to separation is lower and the shock train is longer.

The study described herein refers to isolator/combustion chamber flow interactions in response to transient pressure rise and the corresponding structure of the isolator shock train. Three isolator-entrance Mach numbers were included, 1.6, 1.9, and 2.5, representing operation during the dual-mode combustion and transition to full scramjet mode. The pressure rise is simulated with blockage of the facility exit. The existing shock train pressure rise, hence, its length, prediction indicates a strong dependence on the entrance

Received 29 June 2009; revision received 10 September 2009; accepted for publication 17 September 2009.

*Graduate Research Assistant, Department of Mechanical and Aerospace Engineering. Student Member AIAA.
†Associate Professor, Department of Mechanical and Aerospace Engineering. Associate Fellow AIAA.

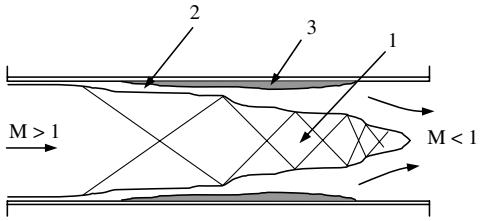

Fig. 1 Schematic of the flowfield in a constant cross-sectional area isolator. The flow is compressed through the oblique shock train in region 1 and through area expansion of the subsonic flow in region 2. A separation forms near the wall in region 3.

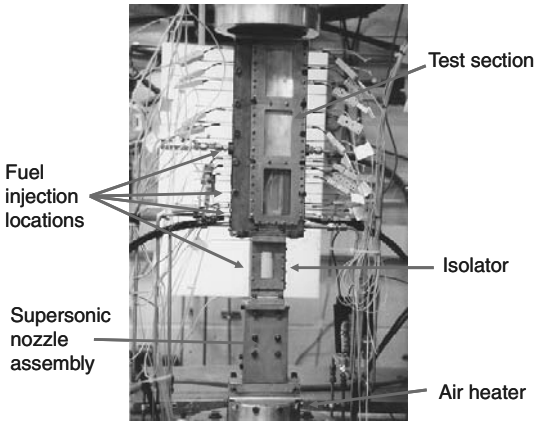

Fig. 2 Supersonic combustion facility.

conditions, that is, the mass and momentum deficit at the combustor entrance and the accurate selection of the wall friction coefficient.

Experimental Setup

The University of Florida supersonic combustion facility, shown in Fig. 2, has been described in detail elsewhere [6]. The facility's is a direct-connect isolator/combustion chamber configuration with a 25×25 mm^2 geometry at the combustion chamber entrance and operates continuously with 0.75 kg/s of airflow heated to 1200 K. It employs a fuzzy logic air temperature control with the capability to simulate transient flight enthalpy and uses interchangeable nozzles to generate combustion chamber entrance Mach numbers from subsonic to 3.6. Six fuel injection locations can be accessed with nonsimilar duels, that is, a combination of gas–gas or gas–liquid fuels. The flowfield of the entire test section and isolator is optically accessible. In addition, a liquid fuel heating capability above 600 K exists.

A two-dimensional flame holder is used here to separate the isolator from the effects of pressure rise in the combustion chamber. The isolator is a constant area duct with a 25×25 mm^2 (1×1 in.^{2}) cross section with a step, h, expansion of 12.5 mm (0.5 in.) on two sides at the combustion chamber entrance.

The pressure rise in the test section was obtained by physically blocking of the test section exit via a mechanism that can modulate the degree of blockage and the rate at which the exit is blocked, thereby simulating fuel transients and the corresponding isolator/combustion chamber flow structure response. A vertical knife edge was used in the schlieren images shown here.

Results

Mach 1.6

Figure 3a shows the flow structure in the isolator and the test section with different blockage levels indicated by the percentage of area reduction, whereas Fig. 3b indicates the corresponding pressure rise. The flow is from left to right in the images. The origin in the pressure plots is placed at the step location, hence, the negative locations for the isolator. The wall pressure distribution is normalized

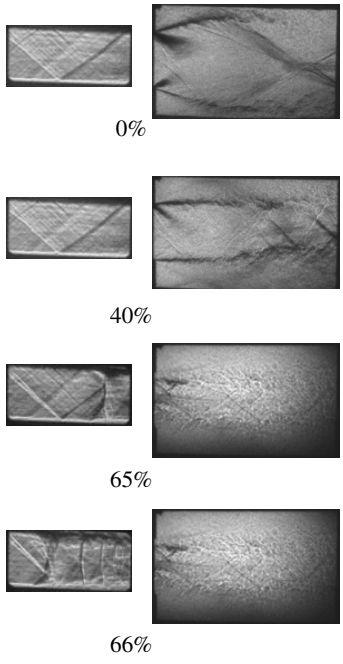

a)

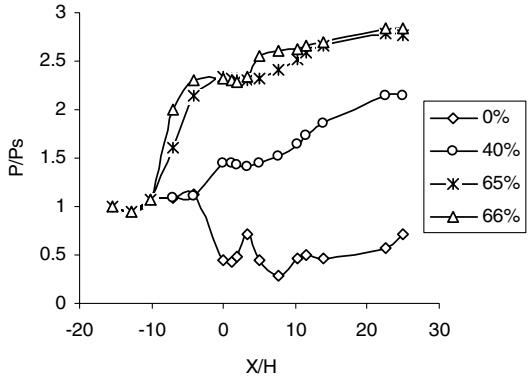

b)

Fig. 3 Mach 1.6. Selected conditions of blockage representing combustion-induced pressure rise showing the upstream interaction penetrating the isolator above a pressure rise of 2.2 in the test section, which corresponds to the thermal choking condition: a) selected schlieren photographs, and b) corresponding pressure ratio.

by the static pressure at the nozzle exit and the axial distance is normalized by the step height.

The pressure increases in the isolator due to the boundary-layer growth. In the absence of any blockage, that is, no heat release, a sharp pressure drop is noted in the base of the step as the flow expands around the corner; then the pressure rises following reattachment at $2.5h$; thereafter, it adjusts to the shock pattern in the combustion chamber.

As the simulated heat release increases through exit area blockage, the shock system adjusts itself, the recirculation region increases substantially, and, as seen in the 40% blockage, it occupies long regions along the combustion chamber walls surrounding the core flow that remain supersonic. The supersonic jet emerging in the surrounding subsonic jet in the test section exhibits "side-to-side" fluctuations that can be attributed to a Coanda effect noticed in bounded flows. The isolator flow is still unaffected until the pressure rises to $P/P_s = 2.2$, which is expected for the thermally chocked condition for $M = 1.6$.

Once the shock train has moved upstream into the isolator, as seen in the 66% blockage case, the typical pattern of shocks in a duct with moderate boundary-layer thickness is observed. The first shock is bifurcated, whereas the subsequent shocks are not. The bifurcated

shock consists of the leading oblique shock, the nearly normal outer shock, and a trailing oblique shock. The outer normal shock is concave facing upstream. A slip line is generated at the bifurcation point and extends downstream. The following shocks are similar but are not bifurcated; the outer region is nearly normal and concave facing downstream [7–9]. Aside from the weak waves that penetrate from the nozzle/isolator interface, caused by a isolator–nozzle slight mismatch, the shock train in the isolator remains symmetric throughout the entire interaction.

The pressure ratio is exceeded as the "heat release" continues and the effects of flow changing in the isolator are noticed in Fig. 3. Above 65% blockage, a clear separation of the boundary layer along the isolator walls is noticed. The test section is almost entirely operating in a subsonic mode. Any further heat release would result, in an actual engine, in upstream effects in the inlet with possible spillage and hammer-shock effects [1].

Mach 1.9

At a higher Mach number, as shown in Fig. 4, and for a significant upstream interaction, the point of bifurcation of the leading shock moves away from the wall and reaches the centerline of the duct. The normal part of the leading shock disappears. The Mach 1.9 case follows a similar trend as the Mach 1.6 case, with the exception that the flow is more resilient to the effects of heat release, the number of shocks increases, and the spacing between two consecutive shocks becomes larger, that is, the interaction region becomes longer. From the pressure plot, the thermal choking is experienced at Mach 1.9 for a pressure ratio rise close to 3. Further "heat release" generates an oblique shock/normal shock train in the isolator duct following separation and establishment of a shock structure bounded by separated regions. The test section becomes entirely subsonic.

Mach 2.5

At Mach 2.5, shown in Fig. 5, continuously increasing the blockage, that is, with more heat release in the test section, the supersonic flow in the combustion chamber resided only along the center surrounded by large subsonic regions. In the isolator the bifurcated shocks are less apparent but the separation increased.

Increasing the blockage to 72.5%, after intersection, the shocks led to large separation regions starting from the leading shocks' origination points. The shocks are more resilient to back pressure and shock bifurcation is not noticed. The separated region increases as well.

Predicted vs Measured Pressure Data

The prediction of pressure rise in the isolator given by Eq. (1) results from the 1-D solution of the equations of motion [10] applied to separated flows. The computation starts at the location where the flow separates and it takes into account mass and momentum deficits at the isolator entrance. The pressure is assumed to grow axially with the dynamic pressure [10].

The 63.5% blockage for the Mach 1.9 case was used as an example with the separation starting at the first pressure port, located at $x/h = -15$ in the facility layout. Figure 6a shows the nozzle exit

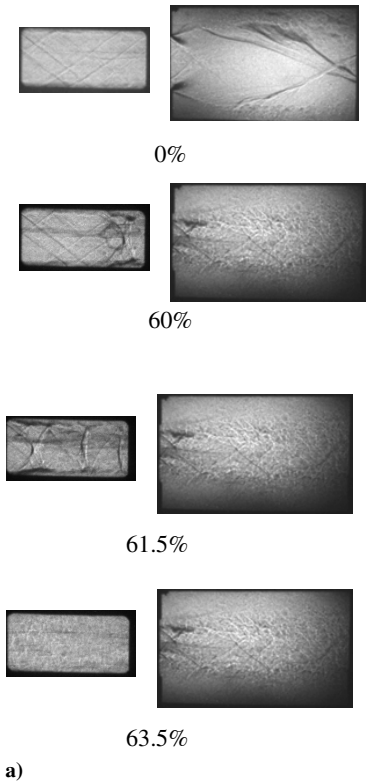

a)

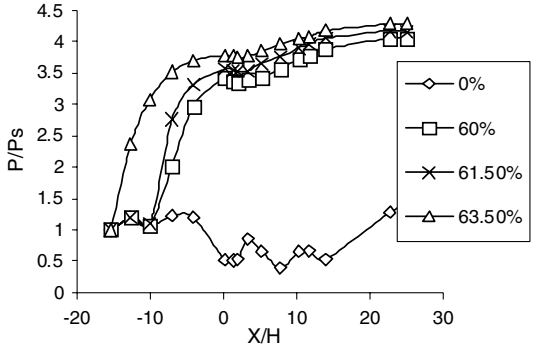

b)

Fig. 4 Mach 1.9. Isolator interaction is noticed when the pressure rises in the combustion chamber: a) selected schlieren photographs, and b) pressure ratio.

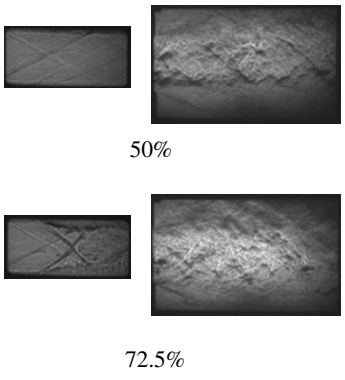

a)

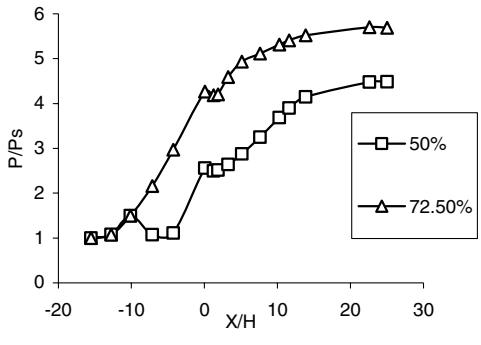

b)

Fig. 5 Mach 2.5. Isolator interaction is noticed when the pressure rises in the combustion chamber: a) selected schlieren photographs, and b) pressure ratio.

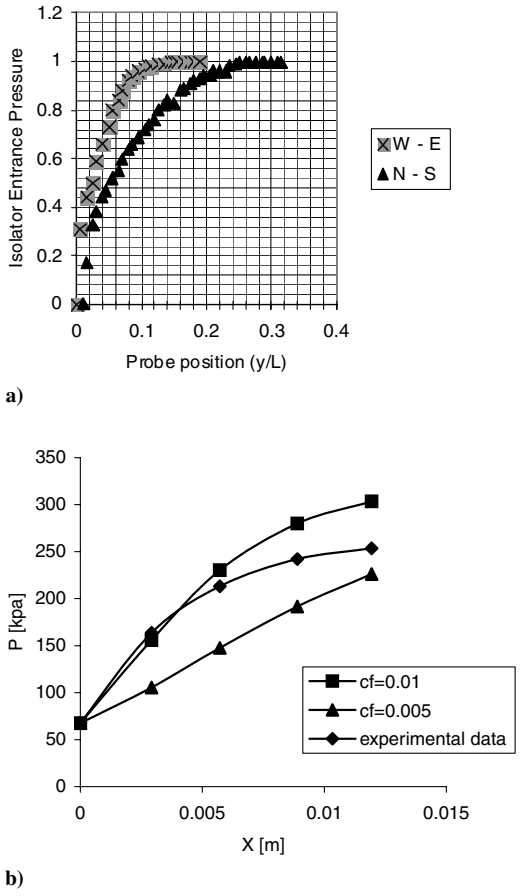

Fig. 6 Isolator pressure rise is strongly influenced by the flow structure emerging from the nozzle: a) nozzle exit boundary layer on the two crossflow directions, and b) predicted vs measured pressure data show the strong influence of the friction coefficient selection.

boundary-layer measurement that was accounted for as the isolator-entrance mass and momentum deficits. Boundary layers are different on the "west–east" side than the "north–south," because only two nozzle sides have compression. Figure 6b shows the predicted vs the measured pressure rise. Two values for the wall friction coefficient were assumed, with $c_f = 0.01$ and 0.005. The analysis shown in Fig. 6b with $c_f = 0.01$ matches the experimental data in the first part of the duct; then, it gradually diverges to a 10% difference at the duct exit. The 0.005 selection underpredicts the pressure rise by as much as 36%. This is a strong effect indicating the sensitivity to the selection of the friction coefficient in a separated flow.

Conclusions

The effects of combustion chamber/isolator interactions were studied experimentally at Mach 1.6, 1.9, and 2.5. At Mach 1.6, the shock train system consists of a series of symmetric, nearly normal shocks. The first shock is bifurcated with incipient separation and is followed by several weaker, secondary, unbifurcated, nearly normal shocks that did not separate the boundary layer. At Mach 1.9, the shock train interaction with the boundary layer is stronger and the point of bifurcation of the leading shock moves away from the wall and reaches the centerline of the duct. The normal part of the leading shock disappears almost entirely At Mach 2.5 the shock train consists of an oblique system with no apparent bifurcated shocks but an increased separation region. Taking into account the correct entrance stream thrust and mass flow rate deficits, the pressure rise was predicted within 10%. The result can be strongly affected by the selection of the friction coefficient.

Acknowledgment

This work has been supported by the Office of Naval Research. We thank Gabriel Roy, the program manager.

References

[1] Segal, C., *The Scramjet Engine: Processes and Characteristics*, Cambridge Univ. Press, Cambridge, England, U.K., 2009, ISBN 052 1838150.

[2] Ortwerth, P. J., "Scramjet Flowpath Integration," *Scramjet Propulsion*, edited by E. T. Curran, and S. N. B. Murthy, Vol. 189, Progress in Astronautics and Aeronautics, AIAA, Reston, VA, 2000, pp. 1105–1293.

[3] Heiser, W. H., and Pratt, D. T., *Hypersonic Airbreathing Propulsion*, AIAA Education Series, AIAA, Washington, DC, 1994.

[4] Matsuo, K., Miyazato, Y., and Kim, H. D., "Shock Train and Pseudo-Shock Phenomena in Internal Gas Flows," *Progress in Aerospace Sciences*, 35, No. 1, Jan. 1999, pp. 33–100. doi:10.1016/S0376-0421(98)00011-6

[5] Waltrup, P. J., and Billig, F. S., "Structure of Shock Waves in Cylindrical Ducts," *AIAA Journal*, Vol. 11, No. 10, 1973, pp. 1404–1408. doi:10.2514/3.50600

[6] Segal, C., and Young, C. D., "Development of an Experimentally Flexible Facility for Mixing-Combustion Interactions in Supersonic Flow," *ASME Transactions. Journal of Tribology*, Vol. 118, No. 2, June 1996, pp. 152–158.

[7] Carroll, B. F., and Dutton, J. C., "Characteristic of Multiple Shock Wave/Turbulent Boundary-Layer Interactions in Rectangular Ducts," *Journal of Propulsion and Power*, Vol. 8, No. 2, 1992, pp. 441–448. doi:10.2514/3.23497

[8] Carroll, B. F., and Dutton, J. C., "Turbulent Phenomena in a Multiple Normal Shock Wave/Turbulent Boundary-Layer Interaction," *AIAA Journal*, Vol. 30, No. 1, 1992, pp. 43–48. doi:10.2514/3.10880

[9] Carroll, B. F., and Dutton, J. C., "Multiple Normal Shock Wave/ Turbulent Boundary-Layer Interactions," *Journal of Propulsion and Power*, Vol. 8, No. 2, 1992, pp. 441–448. doi:10.2514/3.23497

[10] Anderson, G. Y., McClinton, C. R., and Weidner, J. P., "Scramjet Performance," *Scramjet Propulsion*, edited by E. T. Curran, and S. N. B. Murthy, Vol. 189, Progress in Astronautics and Aeronautics, AIAA, Reston, VA, 2000, pp. 369–446.

R. Bowersox
Associate Editor